Supplementary of

Fossil-Dominated SOA Formation in Coastal China: Size-Divergent Pathways of Aqueous Fenton Reactions versus Gas-phase VOC Autoxidation

Jia-Yuan Wang, Meng-Xue Tang, Shan Lu, Ke-Jin Tang, Xing Peng, Ling-Yan He, Xiao-Feng Huang

Key Laboratory for Urban Habitat Environmental Science and Technology, School of Environment and Energy, Peking University Shenzhen Graduate School, Shenzhen, 518055, China.

Correspondence: Meng-Xue Tang (tangmx@pku.edu.cn)

Contents of this file

Text S1- Text S2

Figures S1- Figure S7

Table S1 - Table S3

Text S1:More details of the source apportionment of WSOC by PMF modeling

The data matrices and error matrix of soluble organic carbon (WSOC), organic oxygen (WSOO), CO_2^+, $C_4H_9^+$, and nss-K^+ for a total of 160 samples (16 sets×10 stages) were input into the PMF model. The error matrix was processed according to the signal-to-noise ratio in the ToF-ACSM measurements. Nss-K^+ and CO_2^+ were included in the PMF modeling as tracers of primary biomass-burning organic aerosols (BBOA) and oxygenated organic aerosols (OOA), and $C_4H_9^+$ is a tracer of primary hydrocarbon-like organic aerosols (HOA) or exists in less oxidized organic aerosols as the oxidation product of HOA (Canagaratna et al., 2007; Cao et al., 2018; He et al., 2022; Huang et al., 2020). Two to five factors were tested for modeling, and the three-factor output was found to be the most reasonable solution to explain all identified factor profiles, as will be discussed later; additionally, the solutions with more than three factors did not produce any new meaningful results for WSOC.

The derived EV values of the three-factor solution are shown in Figure S1, where the O/C ratio of each factor was calculated based on the WSOO/WSOC ratio for the factor. The model-input mass of WSOC and the model-reconstructed mass of WSOC exhibited a high correlation (r^2=0.98, slope=1.03). The nss-K^+ was allocated to factor 1, and the O/C ratio of this factor was 0.53; therefore, factor 1 was identified as biomass-burning organic carbon (BBOC). Factor 2 was identified as the more oxidized OOC (MO-OOC) due to its very high O/C ratio (1.85) and the predominant EV of CO_2^+.Almost all $C_4H_9^+$ were allocated to factor 3 and its moderate O/C (0.85); therefore, factor 3 was identified as the less oxidized oxygenated organic carbon (LO-OOC), which is a reasonable result considering that LO-OOC can be partly formed by the oxidation of HOA (Cao et al., 2018).Therefore, it is reasonable to have the three-factor solution above as the most reasonable solution for size-resolved WSOC source apportionment at the study site.

Text S2: The experimental details for the ^{14}C measurements

Equal amounts of water extract of the same stages of MOUDI were combined and concentrated to less than 2 mL by a rotary evaporator and then a freeze drier, and finally titrated onto a quartz filter and placed in a desiccator to dry naturally. The dried filters were used to make graphite samples using the graphitization line at the Guangzhou Institute of Geochemistry, CAS through the hydrogen and zinc reduction method(Xu et al., 2007), and then graphite samples were measured with a compact accelerator mass spectrometry (NEC, National Electrostatics Corporation, USA) at the Guangzhou Institute of Geochemistry, CAS. for analysis of the ratio of $^{14}C/^{12}C$. The fraction of non-fossil carbon (f_{modern}) was calibrated by comparing the measured $^{14}C/^{12}C$ ratio in a sample with that in a modern standard (NBS Oxalic Acid I in AD 1950) and more technical details can be found in the literatures (Zhang et al., 2019; Zhu et al., 2015).

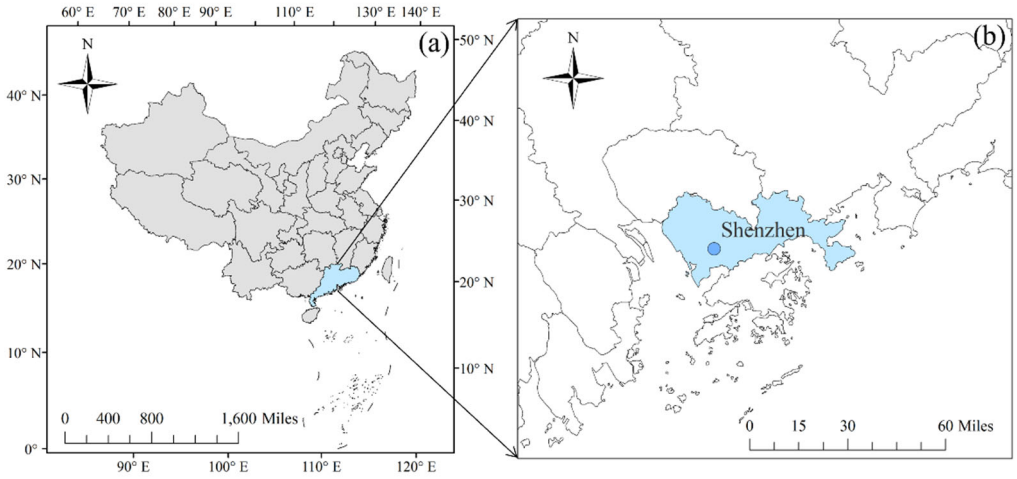

Figure S1. The map of the sampling site in southern China. The blue origin represents the sampling site.

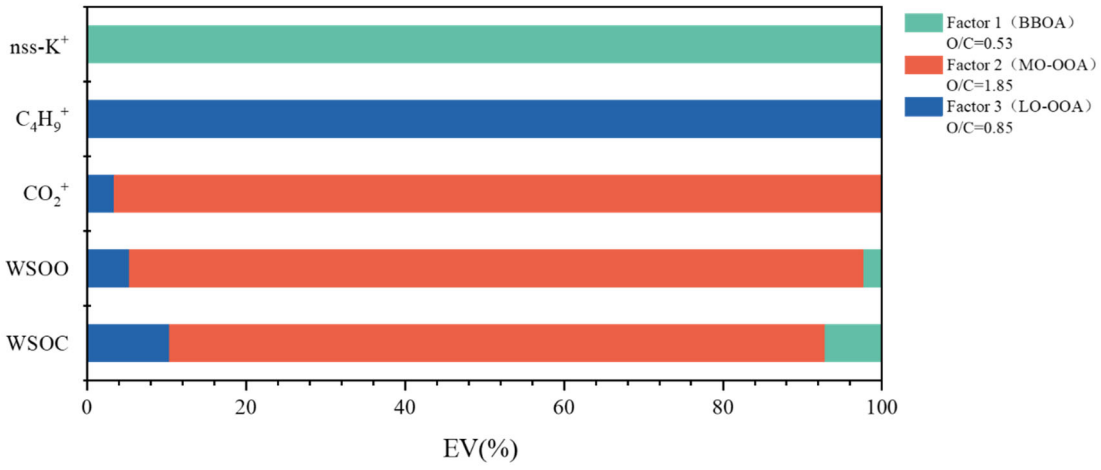

67

68 **Figure S2.** The distribution of EV values for the three-factor solution based on PMF.

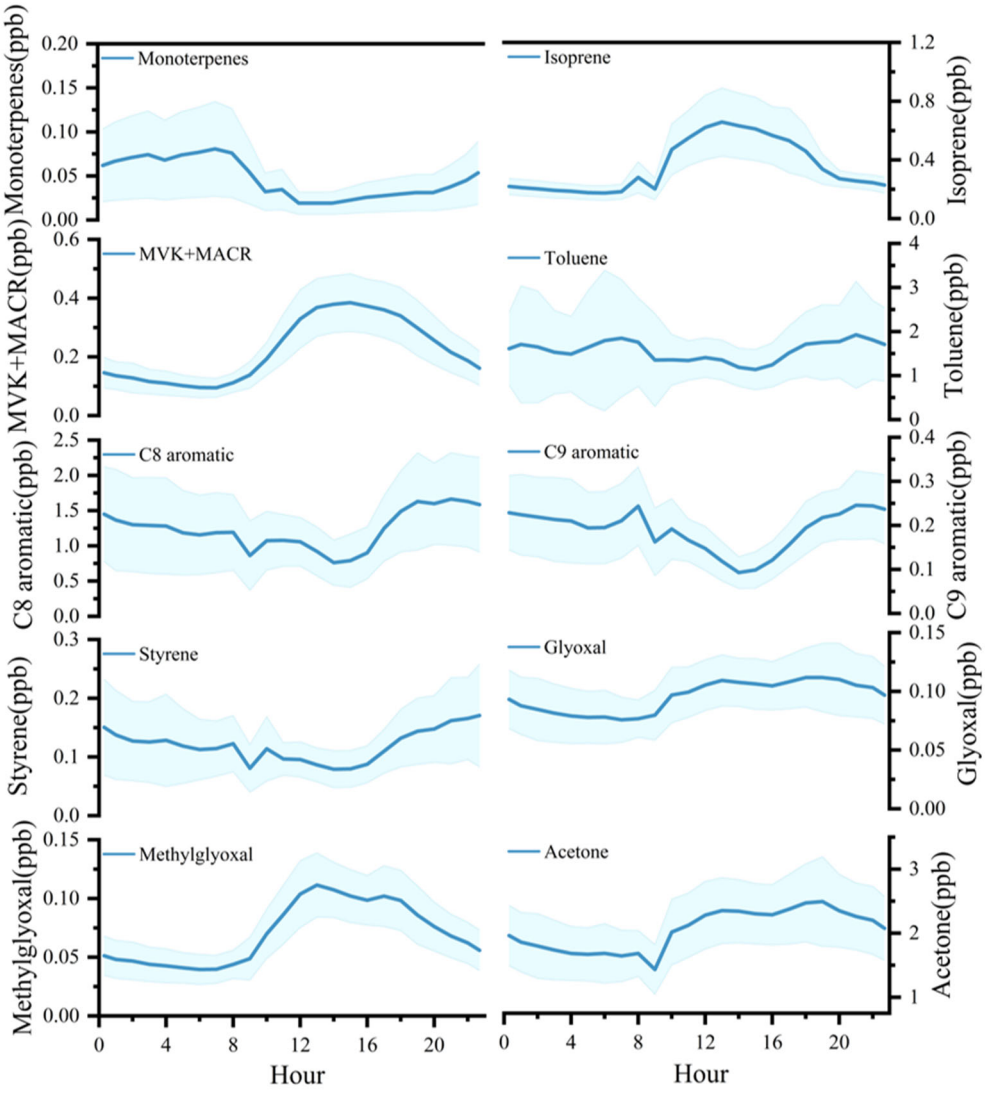

69

70 **Figure S3.** Diurnal variations of 10 selected VOCs during the campaign. Black lines and blue shading

represent the mean and standard deviation, respectively.

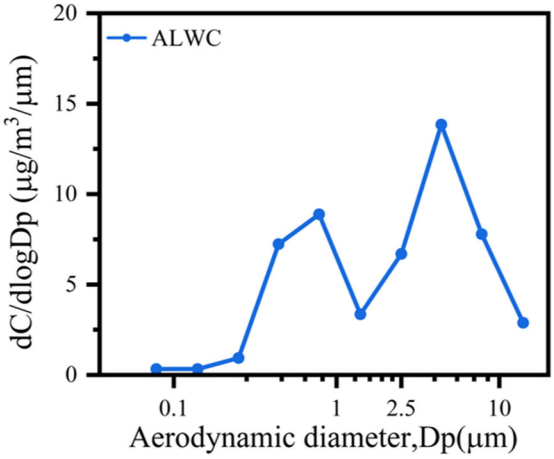

Figure S4. Particle size distribution of ALWC.

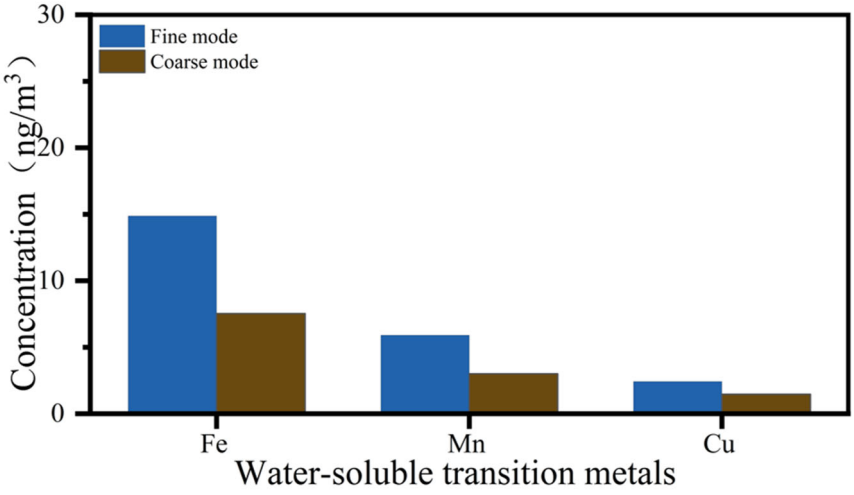

Figure S5. Water-soluble transition metals in the fine and coarse mode.

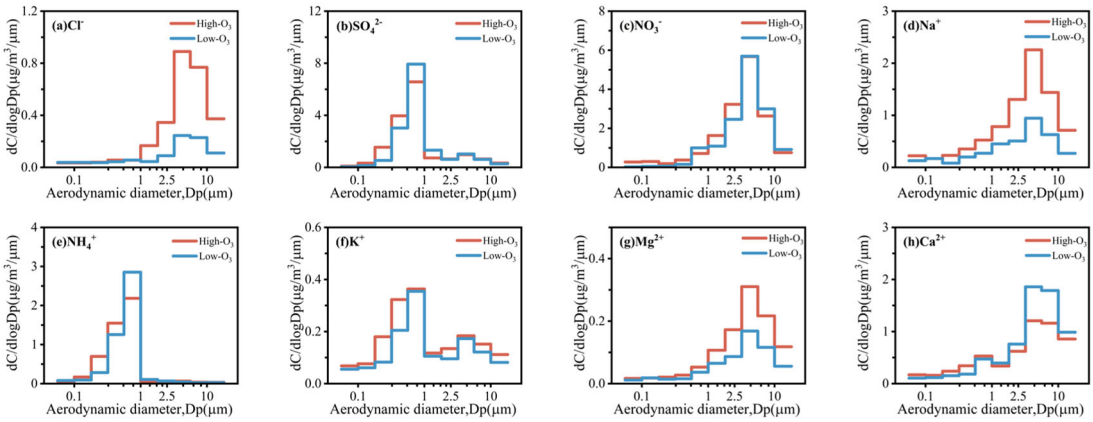

Figure S6. Particle size distribution of inorganic ions during different periods.

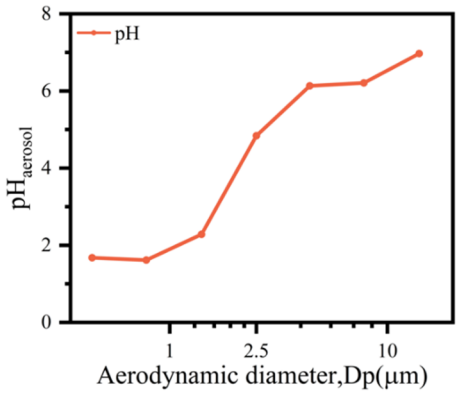

78

79 **Figure S7.** Particle size distribution of $pH_{aerosol}$.

80 **Table S1.** Molecular formula, uncertainty and limits of detection (LOD) of the measured VOCs species

Species	Molecular formula	m/z	Uncertainty	LOD
Monoterpenes	$C_{10}H_{16}$	136.23	9.7%	0.017
Isoprene	C_5H_8	68.06	5.5%	0.030
MVK+MACR	C_4H_6O	71.05	6.1%	0.034
Toluene	C_7H_8	92.06	3.2%	0.090
C8 aromatic	C_8H_{10}	107.13	4.8%	0.009
C9 aromatic	C_9H_{12}	121.15	6.9%	0.030
Styrene	C_8H_8	104.15	5.3%	0.021
Glyoxal	$C_2H_2O_2$	58.04	8.8%	0.017
Methylglyoxal	$C_3H_4O_2$	72.06	4.4%	0.039
Acetone	C_3H_6O	58.04	2.3%	0.150

81 **Table S2.** Summary of mass concentrations of gaseous pollutants (SO_2, NO_x, O_3), PM compositions (PM_1,

82 $PM_{2.5}$, PM_{10}) and meteorological parameters (RH, Temperature (T),WS) during different periods

83 according to this study.

Species	Entire study	High-O_3 period	Low-O_3 period
O_3 (μg/m^3)	68.26	96.52	67.13
NO_x (μg/m^3)	29.20	20.74	27.70
SO_2 (μg/m^3)	6.02	6.37	6.13
PM_1 (μg/m^3)	17.09	14.99	14.96
$PM_{2.5}$ (μg/m^3)	25.21	21.73	22.76
PM_{10} (μg/m^3)	44.10	43.78	41.35
RH (%)	61.27	58.25	72.83
T (°C)	20.0	24.4	24.2
WS (m/s)	0.9	1.2	0.6

84

Table S3. The correlation coefficients between OOC and typical inorganic ions in the campaign. * indicates a significance level of 95% ($p < 0.05$).

	SO_4^{2-}	NH_4^+	K^+	NO_3^-	Cl^-	Ca^{2+}
Fine mode OOC	0.85*	0.80*	0.81*	0.47	0.53	0.34
Coarse mode OOC	0.15	0.26	0.27	0.10	0.16	-0.30

Table S4. The correlation coefficients between OOC and water-soluble metals in the campaign. * indicates a significance level of 95% ($p < 0.05$).

	Cu	Fe	Mn
Fine mode OOC	0.31	0.82*	0.55
Coarse mode OOC	0.64	0.57	0.40

References

Canagaratna, M. R., Jayne, J. T., Jimenez, J. L., Allan, J. D., Alfarra, M. R., Zhang, Q., Onasch, T. B., Drewnick, F., Coe, H., Middlebrook, A., Delia, A., Williams, L. R., Trimborn, A. M., Northway, M. J., DeCarlo, P. F., Kolb, C. E., Davidovits, P., and Worsnop, D. R.: Chemical and microphysical characterization of ambient aerosols with the aerodyne aerosol mass spectrometer, Mass Spectrom. Rev., 26, 185–222, https://doi.org/10.1002/mas.20115, 2007.

Cao, L.-M., Huang, X.-F., Li, Y.-Y., Hu, M., and He, L.-Y.: Volatility measurement of atmospheric submicron aerosols in an urban atmosphere in southern China, Atmospheric Chem. Phys., 18, 1729–1743, https://doi.org/10.5194/acp-18-1729-2018, 2018.

He, D.-Y., Huang, X.-F., Wei, J., Wei, F.-H., Zhu, B., Cao, L.-M., and He, L.-Y.: Soil dust as a potential bridge from biogenic volatile organic compounds to secondary organic aerosol in a rural environment, Environ. Pollut., 298, 118840, https://doi.org/10.1016/j.envpol.2022.118840, 2022.

Huang, X.-F., Dai, J., Zhu, Q., Yu, K., and Du, K.: Abundant Biogenic Oxygenated Organic Aerosol in Atmospheric Coarse Particles: Plausible Sources and Atmospheric Implications, Environ. Sci. Technol., 54, 1425–1430, https://doi.org/10.1021/acs.est.9b06311, 2020.

Xu, X., Trumbore, S. E., Zheng, S., Southon, J. R., McDuffee, K. E., Luttgen, M., and Liu, J. C.: Modifying a sealed tube zinc reduction method for preparation of AMS graphite targets: Reducing background and attaining high precision, Nucl. Instrum. Methods Phys. Res. Sect. B Beam Interact. Mater. At., 259, 320–329, https://doi.org/10.1016/j.nimb.2007.01.175, 2007.

Zhang, X., Li, J., Mo, Y., Shen, C., Ding, P., Wang, N., Zhu, S., Cheng, Z., He, J., Tian, Y., Gao, S., Zhou, Q., Tian, C., Chen, Y., and Zhang, G.: Isolation and radiocarbon analysis of elemental carbon in atmospheric aerosols using hydropyrolysis, Atmos. Environ., 198, 381–386, https://doi.org/10.1016/j.atmosenv.2018.11.005, 2019.

Zhu, S., Ding, P., Wang, N., Shen, C., Jia, G., and Zhang, G.: The compact AMS facility at Guangzhou Institute of Geochemistry, Chinese Academy of Sciences, Nucl. Instrum. Methods Phys. Res. Sect. B Beam Interact. Mater. At., 361, 72–75, https://doi.org/10.1016/j.nimb.2015.06.040, 2015.